Identification of biologically diverse tetrahydronaphtalen-2-ols through the synthesis and phenotypic profiling of chemically diverse, estradiol-inspired compounds

Whitmarsh-Everiss, Thomas; Wang, Zhou; Hansen, Cecilie Hauberg; Depta, Laura; Sassetti, Elisa; Dan, Oliver Rafn; Pahl, Axel; Sievers, Sonja; Laraia, Luca

Published in:
ChemBioChem

Link to article, DOI:
10.1002/cbic.202200555

Publication date:
2023

Document Version
Publisher's PDF, also known as Version of record

ChemBioChem

Research Article
doi.org/10.1002/cbic.202200555

Chemistry Europe
European Chemical Societies Publishing

www.chembiochem.org

Identification of Biologically Diverse Tetrahydronaphthalen-2-ols through the Synthesis and Phenotypic Profiling of Chemically Diverse, Estradiol-Inspired Compounds

Thomas Whitmarsh-Everiss,[a] Zhou Wang,[a] Cecilie Hauberg Hansen,[a] Laura Depta,[a] Elisa Sassetti,[a] Oliver Rafn Dan,[a] Axel Pahl,[b] Sonja Sievers,[b] and Luca Laraia*[a]

Combining natural product fragments to design new scaffolds with unprecedented bioactivity is a powerful strategy for the discovery of tool compounds and potential therapeutics. However, the choice of fragments to couple and the biological screens to employ remain open questions in the field. By choosing a primary fragment containing the A/B ring system of estradiol and fusing it to nine different secondary fragments, we were able to identify compounds that modulated four different phenotypes: inhibition of autophagy and osteoblast differentiation, as well as potassium channel and tubulin modulation. The latter two were uncovered by using unbiased morphological profiling with a cell-painting assay. The number of hits and variety in bioactivity discovered validates the use of recombining natural product fragments coupled to phenotypic screening for the rapid identification of biologically diverse compounds.

Introduction

The synthesis of pseudo-natural products (pseudo-NPs) through the systematic chemical recombination of natural product fragments has recently emerged as a viable strategy for the preparation of compound libraries enriched in biological activity.[1,2] However, the number of possible NP fragment combinations is immense, and the majority of pseudo-NPs published focused on the synthesis of many analogues of one fragment combination only. Therefore, to unlock the full potential of the pseudo-NP concept while maintaining synthetic accessibility within a given library synthesis, a careful balance between the number of fragments combined, as well as the number of analogues for each combination, is required. In this context, we have recently proposed the use of natural product inspired primary fragments, which are suitably functionalized to enable the rapid fusion with up to 15 secondary fragments.[3] Employing this strategy to synthesize three to five analogues per fragment fusion enabled the identification of potent and selective inhibitors of different members of the Aster family of cholesterol transport proteins, where the specific secondary fragment fusion dictated the selectivity for a given sterol transport protein.

The tetrahydronaphthalen-2-ol (THN) fragment is found in over 3000 NPs[4] covering predominantly sterol and terpene NPs but also alkaloids of significant bioactivity. These include estrogens and related estranes as well as morphine and related alkaloids (Figure S1 in the Supporting Information). Despite their undoubted biological importance, the exploration of chemical and biological space around the THN fragment has not been carried out. As such, a systematic synthetic strategy to access diverse secondary fragment fusions to THNs, as well as the biological tools to ascertain the performance diversity of the library and breadth of biological activity,[5] are in demand. To achieve the latter, phenotypic cell-based assays are particularly useful, as they enable the interrogation of a wide array of targets simultaneously.[6] More specifically, image-based morphological profiling strategies such as the cell painting assay (CPA) have been developed to identify biological activity in a more general sense.[7–9] By comparing changes in cellular and organellar morphology upon compound treatment, one can not only determine whether a compound is bioactive, but also whether it is similar to known sets of reference compounds, facilitating mode-of-action and target identification.[10,11]

Herein we describe the synthesis of a diverse compound library containing estradiol's A/B THN ring system fused to nine diverse heterocyclic fragments (Figure 1). Both edge and spirocyclic fusions were accessed, giving a high degree of structural diversity. The resulting library was screened in a range of target and phenotypic assays including the CPA, resulting in the identification of a new tubulin modulating chemotype, new inhibitors of osteoblast differentiation and autophagy, as well as compounds that inhibit potassium channel activators.

[a] Dr. T. Whitmarsh-Everiss, Z. Wang, C. Hauberg Hansen, Dr. L. Depta, Dr. E. Sassetti, O. Rafn Dan, Dr. L. Laraia
Department of Chemistry, Technical University of Denmark
Kemitorvet 207, 2800 Kgs Lyngby (Denmark)
E-mail: luclar@kemi.dtu.dk
[b] Dr. A. Pahl, Dr. S. Sievers
Max Planck Institute of Molecular Physiology
Otto-Hahn-Strasse 11, Dortmund, 44227 (Germany)

Supporting information for this article is available on the WWW under https://doi.org/10.1002/cbic.202200555

This article is part of the Special Collection ChemBioTalents2022. Please see our homepage for more articles in the collection.

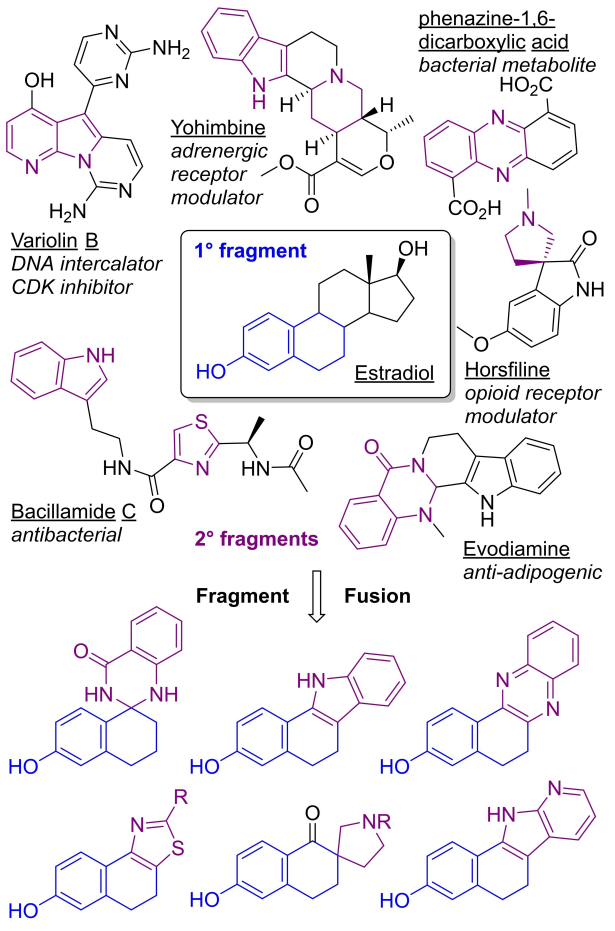

Figure 1. Design principles for the synthesis of a diverse, estrogen-inspired compound library based on the estradiol A/B ring system as a primary fragment, coupled to diverse NP-derived secondary fragments.

Results and Discussion

The synthesis of the compound library began from commercially available methoxytetralone (**1**, Scheme 1). It was reasoned that demethylation to afford the hydroxytetralone (**2**) as the first step would provide a suitable precursor for the library synthesis, as this compound contains the complete A/B ring system found in the estrogens, as well as a ketone handle for further functionalisation.[12] To this effect, **2** was reacted with phenyl hydrazines in a Fischer indole reaction to afford indole-fused THNs **3a–i** in moderate yields. Similarly, reacting **2** with 2-hydrazinopyridines under forcing conditions (di(ethylene glycol), 250 °C under microwave irradiation) afforded 7-azaindoles **4a**, **b**, where the chloro-substituted analogue **4b** oxidized to the fully aromatized system. Quinoline fused THNs **5a–c** were accessed in acceptable yields using a Friedländer quinoline synthesis employing substituted aminoaceto- or benzo-phenones. One analogue was additionally prepared by first performing the Friedländer synthesis from **1**, followed by demethylation (Scheme S1). This afforded the desired product in significantly higher yields, suggesting that inverting the reaction sequence may be beneficial outside of the context of a library synthesis. However, in this specific context the total number of steps to access the whole library would be significantly increased if a demethylation step had to be carried out for every analogue of every fragment fusion. To expand the number and type of available scaffold fusions, α-bromo ketone **6** was synthesized from **2** in good yield. Reacting **6** with phenylenediamines produced quinoxalines **7a**, **b** with concomitant oxidation of the B-ring. Similarly, reaction with thioamides furnished substituted thiazoles **8a–c** in moderate yield. Finally, reacting **6** with aminothiadiazoles resulted in the synthesis of imidazothiadiazoles **9a**, **b**. This scaffold represents the only use of a secondary fragment not found in natural products, which can be considered an expansion of the pseudo-NP concept to include privileged scaffolds not found in nature.[13]

To increase the shape diversity of the compound library, spirocyclic ring fusions were subsequently targeted. Spirocycles increase 3-dimensionality, with documented improvements in physicochemical properties resulting in improved solubility and increased target selectivity.[14,15] From hydroxytetralone **2**, reaction with 2-aminobenzamides in acidic conditions produced spirocyclic dihydroquinazolinones **10a–d** in moderate yield. The reaction proceeds with improved yields from methoxytetralone **1**, confirming the previously observed trend. From **1**, we anticipated that an oxa-Pictet-Spengler reaction[16] with tryptophol would produce spirocycle **11**, however the only product observed was the ring-opened isomer **12**, which is presumably thermodynamically favored owing to the presence of a fully conjugated π system. Finally, synthesis of ester **13** through a Knoevenagel condensation delivered a precursor for a 1,3 dipolar cycloaddition to produce a spirocyclic pyrrolidine-fused scaffold **14** in moderate yield as a single diastereoisomer. With this, the final compound library consisted of 29 compounds featuring nine different fragment fusions.

To assess the biological diversity of our compound library, we profiled it in a range of target-agnostic phenotypic screens. The selected assays included an image-based screen to identify inhibitors of starvation-induced autophagy using MCF7 cells stably transfected with eGFP-tagged LC3 protein.[17] Autophagy is a catabolic cellular recycling process that degrades proteins and regulates nutrient status with autophagy inhibitors having been suggested as potential therapeutics in specific cancer subtypes.[18] Estradiol itself has been reported as an autophagy inducer and inhibitor, a possible result of its pleiotropic effects which vary between different cell models.[19] However selected analogues have also been shown to inhibit autophagy by targeting the transient receptor potential cation channel, mucolipin 1 (TRPML1), and have been optimized for this activity.[20] Here, two compounds from two different fragment fusions (**4a** and **10d**, Table 1 and Figure 2) showed moderate inhibitory activities in the low micromolar range. Both analogues also inhibited autophagy induced by pharmacological inhibition of mTOR using rapamycin (IC_{50} (**4a**) = 6.06 ± 1.05 μM, IC_{50} (**10d**) = 4.36 ± 0.39 μM), suggesting that they act downstream of the mechanistic target of rapamycin (mTOR). Importantly, related analogues were not active, suggesting which structural features are required for activity. Autophagy inhibition was also confirmed by testing the effect of **4a** on

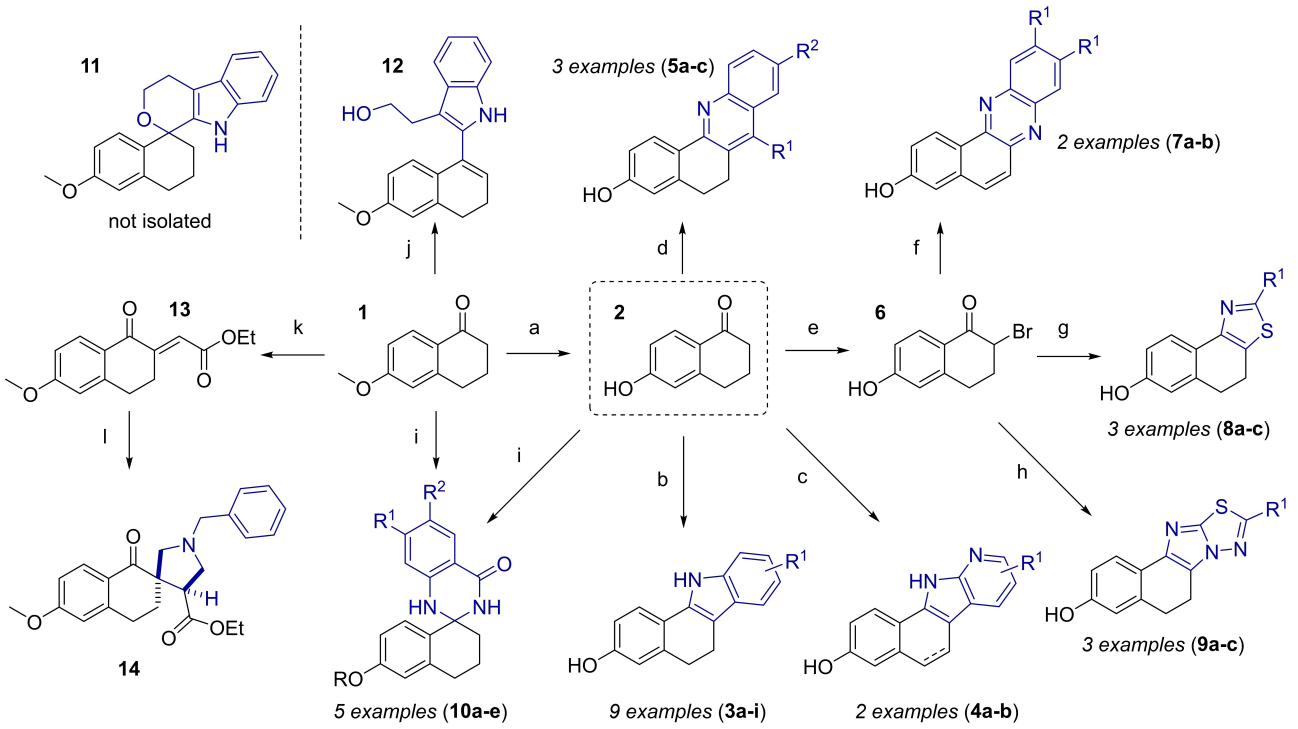

Scheme 1. Synthesis of a diverse, estrogen-inspired compound library. a) HBr, AcOH, 97%; b) Ar-$NHNH_2$, *p*-TsOH, EtOH, reflux, 11–58%; c) py$NHNH_2$, DEG, 250 °C, μW, 7–13%; d) amino aceto- or benzophenone *p*-TsOH, 110 °C, μW, 12–31%; e) $Cu^{II}Br_2$, EtOAc/$CHCl_3$, 80 °C, 60%; f) *o*-phenylenediamines, EtOH, reflux, 4–22%; g) thioamides, EtOH, reflux, 13–34%; h) aminothiadiazoles, EtOH, 150 C, μW, 2–8%; i) 2-aminobenzamides, NH_4Cl, EtOH, reflux, 2–39%; j) tryptophol, SiO_2·TfOH, CH_2Cl_2, 7%; k) ethyl glyoxylate, *p*-TsOH, $MgSO_4$, toluene, reflux, 25%; l) *N*-(methoxymethyl)-*N*-(trimethylsilylmethyl)benzylamine, TFA, CH_2Cl_2, 24%.

LC3-II levels by western blot, which showed a small but detectable dose-dependent decrease in LC3-II levels (Figure S2).

The library was also screened for inhibition of hedgehog (Hh) signaling. For this purpose, an osteoblast differentiation assay was initially used, with purmorphamine as a smoothened agonist to activate the Hh pathway, leading to the expression of alkaline phosphatase, the activity of which is ultimately measured.[21] Surprisingly, a diverse set of library compounds inhibited osteogenesis, including unsubstituted indole **3a**, quinoxaline **7b**, and two imidazothiadiazoles **9a** and **9c** (Table 1). Importantly, none of the compounds inhibited cell growth in the same cell line, which can be a common source of false positives (data not shown). Thioether **9a** was particularly potent with an $IC_{50}=0.32$ μM, which is only four-fold less than the clinically approved drug vismodegib in the same assay ($IC_{50}=0.07$ μM), suggesting that it may be a suitable candidate for further optimization. To determine whether compounds were direct inhibitors of hedgehog signaling, the whole library was tested in a gene reporter assay specifically monitoring hedgehog signaling, as well as in a secondary assay monitoring direct alkaline phosphatase activity. Surprisingly, all compounds were inactive in both assays, suggesting that they are inhibitors of osteoblast differentiation that do not inhibit either hedgehog signaling or alkaline phosphatase (Table S1 in the Supporting Information Table S1). Therefore, the direct targets of these compounds remain to be determined.

To assess biological activity in a more general and pathway-agnostic manner and predict potential targets of the compound library members, all compounds were also screened at three concentrations (10, 30 and 50 μM) in the cell painting assay.[22] Biological activity was measured by an induction value, which represents the percentage of features that were significantly altered compared to a DMSO control. Seventeen out of twenty nine (59%) compounds had an induction value of >5% at either 10 or 30 μM, confirming the library had a high degree of bioactivity overall (Table 1).[23] It has previously been shown that the cell painting assay can predict certain modes-of-action with high confidence, including lysosomotropism,[10,11] mitochondrial respiratory activity,[16,24] and modulation of tubulin polymerization.[25] This is due to the availability of reference compounds that closely cluster in relation to their biological fingerprint in the CPA.[26] Intriguingly, several compounds in our libraries showed high biological similarity to reference clusters. Four spirocyclic dihydroquinazolinones showed similarity to tubulin modulators (Figure 3a, b). The similarity in the biological profiles can also be visualized clearly using uniform manifold approximation and projection (UMAP) plots (Figure 3c). Here, tubulin modulators define a larger area with spiro-dihydroquinazolinones interspersed throughout. Notably, estradiol and several derivatives have previously been reported to inhibit tubulin polymerization, and show the same fingerprint in the CPA.[27] Interestingly, dihydroquinazolinone **10d** was also a hit in the autophagy assay. This result suggests that autophagy inhibition may be a result of interference with microtubule dynamics. This would confirm the previously reported association between microtubule integrity and autophagosome for-

Table 1. Assessment of the biological activity of the compound library.[a]

Cmpd	Starvation-induced autophagy IC_{50} [μM]	Osteoblast differentiation assay (ODA) IC_{50} [μM]	Induction value at 30 μM, cell painting assay [%]
3a	>10	**3.65±0.56**	10
3b	>10	>10	19
3c	>10	>10	11
3d	>10	>10	12
3e	>10	>10	70
3f	>10	>10	16
3g	>10	>10	27
3h	>10	>10	nt
3i	>10	>10	14
4a	**3.1±0.14**	>10	31*
4b	>10	>10	11*
5a	>10	>10	14
5b	>10	>10	1
5c	>10	>10	0
7a	>10	>10	10
7b	>10	**5.88±0.50**	0
8a	>10	>10	0
8b	>10	>10	0
8c	>10	>10	14
9a	>10	**0.32±0.27**	2
9b	>10	>10	nt
9c	>10	**9.16±0.76**	1
10a	>10	>10	0
10b	>10	>10	3
10c	>10	>10	12
10d	**1.87±0.06**	>10	25
10e	>10	>10	36
12	>10	>10	5
14	>10	>10	2

[a] All data are shown as the mean±SEM of three independent experiments unless otherwise specified. *Data in the CPA at 10 μM. nt=not tested. Please see main text and Supporting Information for detailed descriptions of the individual assays.

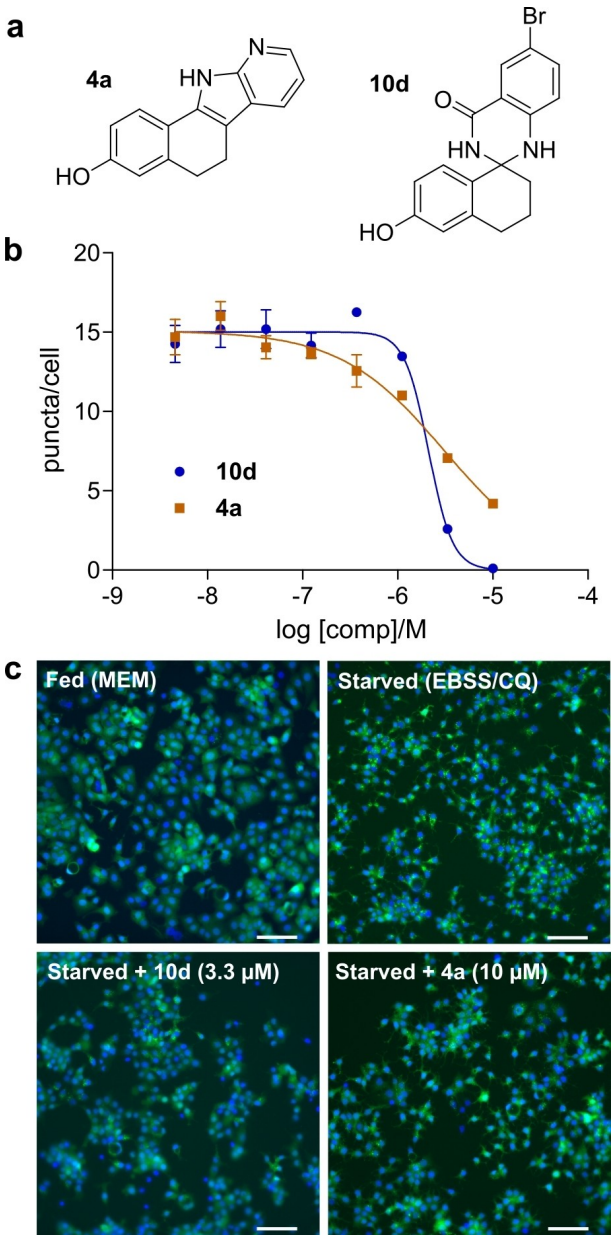

Figure 2. Inhibition of autophagy by estrogen-inspired compounds. a) Structures of active compounds. b) Dose–response curves of inhibitory activity of compounds **4a** and **10d** in an MCF7 cell line stably expressing eGFP-LC3; $n=3$, data shown as the mean±SEM of an experiment carried out in triplicate. c) Representative images used in the quantification of data shown in (b). Scale bar: 110 μm.

mation and fusion, particularly under starvation conditions such as those employed in our assay.[28,29] Compounds **10b** and **10d** were subsequently confirmed to inhibit tubulin polymerization in an in vitro assay using purified tubulin, where both were less active than the reference compound nocodazole (Figure 3d).

Furthermore, five indole fusions showed biological similarity to two different potassium channel activators, flindokalner (BMS-204352) and NS309, which themselves have different selectivities across a range of channels (Figure 3a and e).[30,31] In the UMAP plot, the potassium channel modulators define a narrower area, with indole-fused analogues appearing in their vicinity (Figure 3c). The ability of the cell painting assay to detect changes in cellular morphology imparted by ion channel modulation had not been reported previously, and defines a new area for future analysis. Importantly, estradiol itself has been reported to inhibit calcium activated potassium channels KCNQ2/3 (K_v7.2/7.3),[32] while being an activator of the big potassium (BK or K_{Ca}1.1) channels.[33] To complicate matters, estradiol and derivatives have also been shown to regulate potassium channels at the transcriptional level, most likely through effects on the estrogen receptor.[34] To verify whether our indole-fused THNs could modulate calcium-activated potassium channels more generally, we first tested **3i** in a voltage-gated potassium channel (K_v) binding assay using [^{125}I] radiolabeled α-dendrotoxin. Here, we observed that **3i** dose-dependently inhibited binding (Figure 3f). To see whether the compounds exhibited any functional activity at K_v7.2/7.3, they were tested as potential agonists in a cell line expressing both receptors. While **3e** and **3i** induced weak receptor activation (Figure S3), they were an order of magnitude less potent than the control compound Retigabine, suggesting that activity at K_v7.2/7.3 is not the main source of the phenotype observed in the CPA. Further work exploring activity of these compounds at other potassium channels is ongoing.

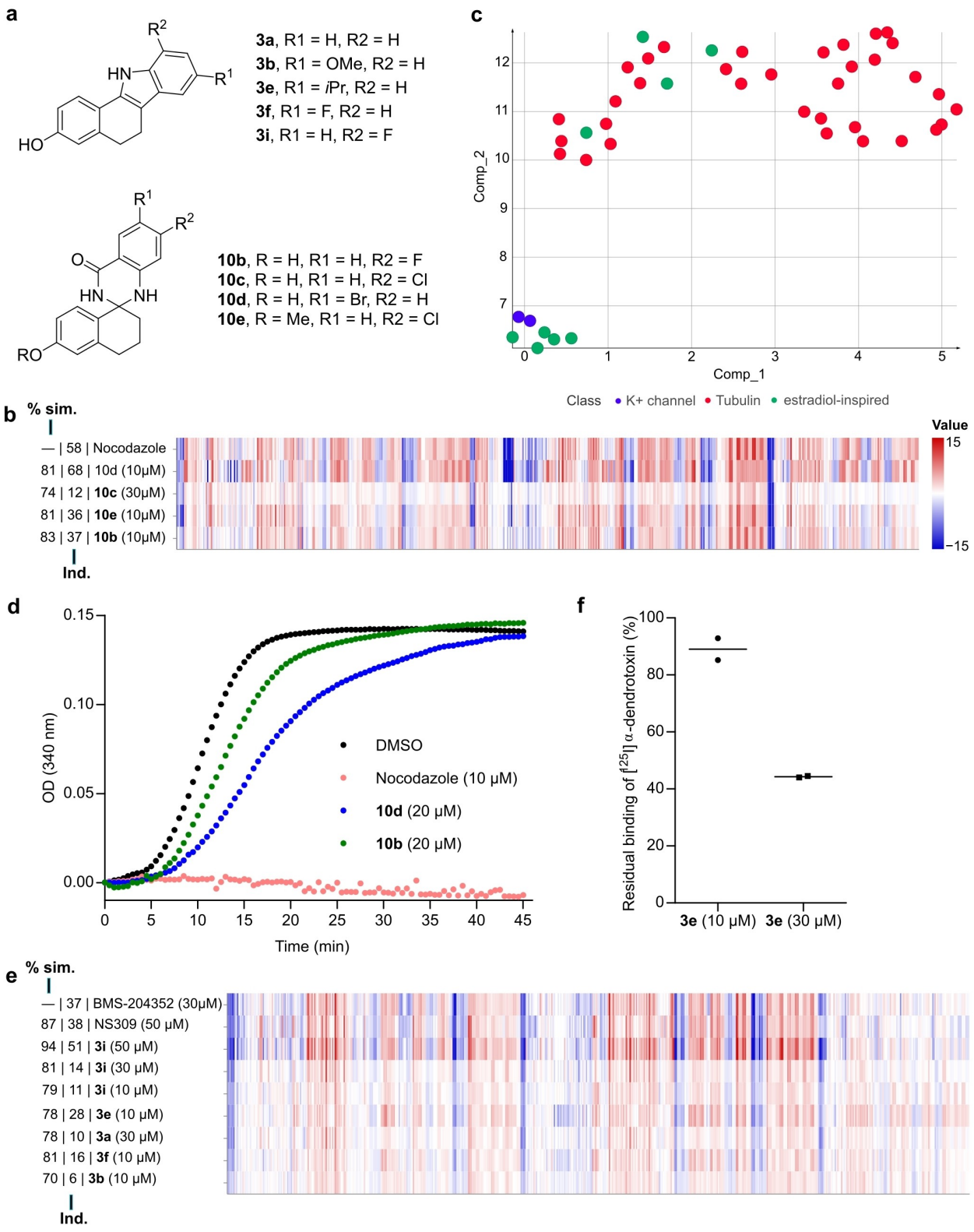

Figure 3. Profiling of estradiol-inspired compounds in the cell-painting assay. a) Structures of compounds with biological similarity to known reference compounds. b) Comparison of morphological fingerprints induced by the known anti-mitotic Nocodazole and the test compounds **10b–e**; Ind. = % induction, % sim. = % similarity to the first reference compound. c) Uniform manifold approximation and projection (UMAP) analysis for comparison between test and refence compounds displayed in (a)–(c); non-normalized data, 7 neighbors. d) Tubulin polymerization inhibitory activity of **10b** and **10d**. Data from a representative experiment. Nocodazole was used as a positive control. e) Comparison of the morphological fingerprints induced by the known potassium channel activators BMS-204352 and NS309 and the test compounds **3a**, **b**, **e**, **f** and **I**. f) Inhibition of [^{125}I] radiolabeled α-dendrotoxin binding to rat potassium channels by **3e**. Data are the mean of an experiment carried out in duplicate.

Finally, to exclude that any of the biological activity for the compound library was correlated to activity at the estrogen receptor (ER), we carried out an in vitro ERα fluorescence polarization (FP) assay (Figure S4). Most of the compounds were completely inactive at 10 μM, with only five showing low levels of inhibition (~40% at 10 μM). This can be attributed to the loss of the second hydrogen bond donor present in estradiol, but absent in all of the library compounds. This finding further strengthens the previously observed notion that synthesizing unprecedented fusions of natural product fragments leads to compounds with biological activity, which deviates from the primary target of the guiding natural products themselves.

Conclusions

In conclusion, we have developed a general synthetic strategy to access diverse pseudo-natural products containing an estradiol-inspired primary fragment fused to a range of secondary fragments. Edge and spirocyclic fusions were successfully targeted, giving rise to nine structurally diverse scaffolds. Biological profiling in cell-based screens produced hits in all of the phenotypes tested. Importantly, the compound's activities were mostly orthogonal to each other; this validates the strategy to target diverse NP fragment fusions. In fact, five of the nine scaffold fusions synthesized showed diverse activity such as autophagy inhibition (azaindole fusion), osteogenesis inhibition (imidazothiadiazole and quinoxaline fusion), and similarity to potassium channel activators (indole fusion) and tubulin modulators (spirocyclic dihydroquinazolinone fusion). All phenotypes modulated can be traced back to the activity of the parent natural product estradiol, which is known to depolymerize microtubules at high concentrations and regulate osteogenesis, as well as being involved in the regulation of calcium-activated potassium channels. However, we could show that varying the secondary fragment drastically changes the biological activity, thus suggesting that selectivity for a given biological process can be obtained even when starting from a relatively promiscuous primary fragment. This is in line with our own work on sterol transport proteins, where the fusion of a primary steroidal fragment to diverse secondary fragments provided selective modulators of individual sterol transport proteins.[3] This new work reinforces this concept and shows that the same selectivity can be identified even when screening phenotypically, rather than in a target-based approach. In summary our results validate the pseudo-natural product design strategy for the production of chemically and biologically diverse compounds enriched in bioactivity, and phenotypic assays including the CPA as tools to rapidly identify and categorize them.

Experimental Section

Synthetic procedures and associated data and spectra to access all library compounds can be found in the Supporting Information.

Osteoblast differentiation assay: Mouse embryonic mesoderm fibroblast C3H10T1/2 cells were used to monitor osteoblast differentiation. These multipotent mesenchymal progenitor cells differentiate into osteoblasts upon treatment with the SMO agonist Purmorphamine.[35] During differentiation osteoblast specific genes such as alkaline phosphatase (ALK), which plays an essential role in bone formation, are highly expressed. Activity of ALK can directly be monitored by following substrate hydrolysis yielding a highly luminescent product. Inhibition of the pathway results in reduction of luminescence. The screening for small molecule inhibitors of the Hh pathway was carried out in 384 well format. 800 cells per well were seeded and allowed to grow overnight. The next day, compounds were added to a final concentration of 10 μM using the acoustic nanoliter dispenser ECHO 520. After 1 h, Purmorphamine was added to a final concentration of 1.5 μM; control cells did not receive Purmorphamine. After four days, the cell culture medium was aspirated and a commercial luminogenic ALK substrate (CDP-Star, Roche) was added. After 1 h, luminescence was read. To identify and exclude toxic compounds that also lead to a reduction in the luminescent signal, cell viability measurements were carried out in parallel. The cell viability assay followed the same workflow as the osteoblast differentiation assay, except that only 200 cells per well were seeded. Cell culture medium alone served as control for the cell viability assay. For the measurement of cell viability, Cell Titer Glo reagent (Promega) which determines the cellular ATP content was used. Hits were scored as showing at least a 50% reduction in the luminescent signal in the HH assay, and a minimum of 80% cell viability. Dose–response analysis for hit compounds in this assay and all others described was done using a threefold dilution curve starting from 10 μM. IC_{50} values were calculated using the Quattro software suite (Quattro Research GmbH).

Screening for autophagy modulators: MCF7-GFP-LC3 (4000 cells/well) cells were seeded in 384 well plates (Greiner) and incubated overnight at 37 °C and 5% CO_2. The next day cells were washed three times with 1× PBS using plate washer ELX405 (Biotek). Following this, 10 μM of compound was added using Echo dispenser (Labcyte) along with EBSS (starvation medium) and Chloroquine (50 μM) or Rapamycin (100 nM) and Chloroquine (50 μM). Three hours after incubation at 37 °C cells were fixed by addition of 25 μL formaldehyde in 1× PBS (4.6% final concentration) and simultaneously staining the nucleus with 1:500 Hoechst (Stock 1 mg mL^{-1}) for 20 min at RT. Fixed cells were washed thrice with 1× PBS using plate washer ELX405 (Biotek). For visualization 4 pictures/well were acquired using ImageXpress Micro XL (Molecular Devices) at 20× and analyzed with the granularity algorithm of MetaXpress Software (Molecular Devices).

Cell-painting assay: The described assay closely follows the method described by Bray et al.[7] Initially, 5 μL U2OS medium were added to each well of a 384-well plate (PerkinElmer CellCarrier-384 Ultra). Subsequently, U2OS cells were seeded with a density of 1600 cells per well in 20 μL medium. The plate was incubated for 10 min at ambient temperature, followed by an additional 4 h of incubation (37 °C, 5% CO_2). Compound treatment was performed with the Echo 520 acoustic dispenser (Labcyte) at final concentrations of 50, 30, or 10 μM. Incubation with compound was performed for 20 h (37 °C, 5% CO_2). Subsequently, mitochondria were stained with Mito Tracker Deep Red (Thermo Fisher Scientific, cat. no. M22426). The Mito Tracker Deep Red stock solution (1 mM) was diluted to a final concentration of 100 nM in prewarmed medium. The medium was removed from the plate leaving 10 μL residual volume and 25 μL of the Mito Tracker solution were added to each well. The plate was incubated for 30 min in darkness (37 °C, 5% CO_2). To fix the cells 7 μL of 18.5% formaldehyde in PBS were added, resulting in a final formaldehyde concentration of 3.7%. Subsequently, the

plate was incubated for another 20 min in darkness (RT) and washed three times with 70 μL of PBS (Biotek Washer Elx405). Cells were permeabilized by addition of 25 μL 0.1% Triton X-100 to each well, followed by 15 min incubation (RT) in darkness. The cells were washed three times with PBS leaving a final volume of 10 μL. To each well 25 μL of a staining solution were added, which contains 1% BSA, 5 μL/mL Phalloidin (Alexa594 conjugate, Thermo Fisher Scientific, A12381), 25 μg/mL Concanavalin A (Alexa488 conjugate, Thermo Fisher Scientific, cat. no. C11252), 5 μg/mL Hoechst 33342 (Sigma, cat. no. B2261-25 mg), 1.5 μg/mL WGA-Alexa594 conjugate (Thermo Fisher Scientific, cat. no. W11262) and 1.5 μM SYTO 14 solution (Thermo Fisher Scientific, cat. no. S7576). The plate was incubated for 30 min (RT) in darkness and washed three times with 70 μL PBS. After the final washing step, the PBS was not aspirated. The plates were sealed and centrifuged for 1 min at 500 rpm. The plates were prepared in triplicates with shifted layouts to reduce plate effects and imaged using a Micro XL High-Content Screening System (Molecular Devices) in 5 channels (DAPI: Ex350-400/Em410-480; FITC: Ex470-500/Em510-540; Spectrum Gold: Ex520-545/Em560-585; TxRed: Ex535-585/Em600-650; Cy5: Ex605-650/Em670-715) with 9 sites per well and 20× magnification (binning 2).

The generated images were processed with the *CellProfiler* package (https://cellprofiler.org/, version 3.0.0) on a computing cluster of the Max Planck Society to extract 1716 cell features per microscope site. The data were then further aggregated as medians per well (9 sites→1 well), then over the three replicates. Further analysis was performed with custom *Python* (https://www.python.org/) scripts using the *Pandas* (https://pandas.pydata.org/) and *Dask* (https://dask.org/) data processing libraries as well as the *Scientific Python* (https://scipy.org/) package. From the total set of 1716 features, a subset of highly reproducible and robust features was determined using the procedure described by Woehrmann et al.[36] in the following way:

Two biological repeats of one plate containing reference compounds were analyzed. For every feature, its full profile over each whole plate was calculated. If the profiles from the two repeats showed a similarity $>=0.8$ (see below), the feature was added to the set. This procedure was only performed once and resulted in a set of 579 robust features out of the total of 1716 that was used for all further analyses.

The phenotypic profiles were compiled from the *Z*-scores of all individual cellular features, where the *Z*-score is a measure of how far away a data point is from a median value. Specifically, *Z*-scores of test compounds were calculated relative to the median of DMSO controls. Thus, the *Z*-score of a test compound defines how many median absolute deviations (MADs) the measured value is away from the median of the controls as illustrated by the following formula:

$$z\_score = \frac{value_{meas.} - Median_{Controls}}{MAD_{Controls}}$$

The phenotypic compound profile is then determined as the list of *Z*-scores of all features for one compound. In addition to the phenotypic profile, an induction value was determined for each compound as the fraction of significantly changed features, in percent:

$$Induction\ [\%] = \frac{number\ of\ features\ with\ abs.\ values > 3}{total\ number\ of\ features}$$

Similarities of phenotypic profiles were calculated from the correlation distances between two profiles (https://docs.scipy.org/doc/scipy/reference/generated/scipy.spatial.distance.correlation.html; Similarity = 1-correlation distance).

Tubulin polymerization assay: A tubulin solution (5 mg mL^{-1}) was prepared by dissolving porcine α/β-tubulin (99% pure, Cytoskeleton, USA) in 1× General Tubulin Buffer (80 mM Na-PIPES pH 6.9, 1 mM $MgCl_2$ and 1 mM EGTA, 10% glycerol). In total 100 μL of this tubulin solution was combined with test compounds dissolved in DMSO to give the desired final concentration, and incubated for 30 min. To this was added GTP to a final concentration of 1 mM to start the polymerisation reaction. Tubulin polymerization was monitored by measuring the increase in absorbance at 340 nm in an Infinite M200 plate reader (Tecan).

Potassium channel binding and functional assays: These assays were performed by the commercial supplier Eurofins/Cerep. Non-specific binding to the rat potassium ion channels was performed using the K_V (non-selective) rat potassium ion channel [^{125}I] α-dendrotoxin binding assay (item 166), at Cerep.[37] In brief, membrane homogenates of cerebral cortex (8 μg protein) are incubated for 60 min at 22 °C with 10 pM [^{125}I]-dendrotoxin in the absence or presence of the test compound in a buffer containing 50 mM Tris·HCl (pH 7.4), 140 mM NaCl, 5 mM KCl, 1.3 mM $MgSO_4$ and 0.1% BSA. Following incubation, the samples are filtered rapidly under vacuum through glass fiber filters (GF/B, Packard) presoaked with 0.3% PEI and rinsed several times with ice-cold 50 mM Tris·HCl (pH 7.4) using a 96-sample cell harvester (Unifilter, Packard). The filters are dried then counted for radioactivity in a scintillation counter (Topcount, Packard) using a scintillation cocktail (Microscint 0, Packard). The results are expressed as a percent inhibition of the control radioligand specific binding.

Functional activity at the K_v7.2/7.3 channels was performed using the hK_v7.2/7.3 potassium channel agonist assay (item CYL8059QB3), at Eurofins. The automated whole cell patch-clamp (Qube 384) technique is used to record outward K^+ currents. This is carried out in CHO cells expressing the human K_v7.2/7.3 channels. The cells are harvested by Accutase and maintained in serum-free medium (HEK 293 SFM) at room temperature before assay. On the instrument the cells are pipetted into each well of a 384-well plate in external solution. After whole cell configuration is achieved, the cell is held at −120 mV. Then the cell is depolarized from −120 to +30 mV in 10 mV increment for 1 s and then back to −120 mV for 500 ms. This paradigm is delivered once every 20s to monitor the current amplitude and determine current-voltage relationship before and after compound addition. The cells are incubated with each test concentration for 5 min. The assays were conducted at room temperature.

Acknowledgements

Research in the Laraia Lab is supported by the Novo Nordisk Foundation (NNF19OC0055818 and NNF21OC0067188), the Carlsberg foundation (CF19-0072), Independent Research Fund Denmark (9041-00241B and 9041-00248B) and DTU. S. S. and A. P. acknowledge the Max Planck Society for funding.

Conflict of Interest

The authors declare no conflict of interest.

Data Availability Statement

The data that support the findings of this study are available in the supplementary material of this article.

Keywords: cell painting assay · estradiol · mode-of-action · pseudo-natural products · target identification

[1] G. Karageorgis, D. J. Foley, L. Laraia, H. Waldmann, *Nat. Chem.* **2020**, *12*, 227–235.
[2] G. Karageorgis, D. J. Foley, L. Laraia, S. Brakmann, H. Waldmann, *Angew. Chem. Int. Ed.* **2021**, *60*, 15705–15723; *Angew. Chem.* **2021**, *133*, 15837–15855.
[3] T. Whitmarsh-Everiss, A. H. Olsen, L. Laraia, *Angew. Chem. Int. Ed.* **2021**, *60*, 26755–26761; *Angew. Chem.* **2021**, *133*, 26959–26965.
[4] "Dictionary of Natural Products 30.2," can be found under http://dnp.chemnetbase.com.
[5] I. Pavlinov, E. M. Gerlach, L. N. Aldrich, *Org. Biomol. Chem.* **2019**, *17*, 1608–1623.
[6] L. Laraia, L. Robke, H. Waldmann, *Chem* **2018**, *4*, 705–730.
[7] M.-A. Bray, S. Singh, H. Han, C. T. Davis, B. Borgeson, C. Hartland, M. Kost-Alimova, S. M. Gustafsdottir, C. C. Gibson, A. E. Carpenter, *Nat. Protoc.* **2016**, *11*, 1757–1774.
[8] J. C. Caicedo, S. Cooper, F. Heigwer, S. Warchal, P. Qiu, C. Molnar, A. S. Vasilevich, J. D. Barry, H. S. Bansal, O. Kraus, M. Wawer, L. Paavolainen, M. D. Herrmann, M. Rohban, J. Hung, H. Hennig, J. Concannon, I. Smith, P. A. Clemons, S. Singh, P. Rees, P. Horvath, R. G. Linington, A. E. Carpenter, *Nat. Methods* **2017**, *14*, 849–863.
[9] E. B. Svenningsen, T. B. Poulsen, *Bioorg. Med. Chem.* **2019**, *27*, 2609–2615.
[10] L. Laraia, G. Garivet, D. J. Foley, N. Kaiser, S. Müller, S. Zinken, T. Pinkert, J. Wilke, D. Corkery, A. Pahl, S. Sievers, P. Janning, C. Arenz, Y. Wu, R. Rodriguez, H. Waldmann, *Angew. Chem. Int. Ed.* **2020**, *59*, 5721–5729; *Angew. Chem.* **2020**, *132*, 5770–5778.
[11] T. Schneidewind, A. Brause, B. Schölermann, S. Sievers, A. Pahl, M. G. Sankar, M. Winzker, P. Janning, K. Kumar, S. Ziegler, H. Waldmann, *Cell Chem. Biol.* **2021**, *28*, 1780–1794.e5.
[12] D. J. Foley, H. Waldmann, *Chem. Soc. Rev.* **2022**, *51*, 4094–4120.
[13] F. Alonso, A. Galilea, P. A. Mañez, S. L. Acebedo, G. M. Cabrera, M. Otero, A. A. Barquero, J. A. Ramírez, *ChemMedChem* **2021**, *16*, 1945–1955.
[14] F. Lovering, *MedChemComm* **2013**, *4*, 515–519.
[15] K. Hiesinger, D. Dar'In, E. Proschak, M. Krasavin, *J. Med. Chem.* **2021**, *64*, 150–183.
[16] A. Burhop, S. Bag, M. Grigalunas, S. Woitalla, P. Bodenbinder, L. Brieger, C. Strohmann, A. Pahl, S. Sievers, H. Waldmann, *Adv. Sci.* **2021**, *8*, 1–10.
[17] G. Konstantinidis, S. Sievers, Y.-W. Wu, in *Autophagy in Differentiation and Tissue Maintenance: Methods and Protocols* (Ed.: K. Turksen), Springer, New York, **2019**, pp. 187–195.
[18] T. Whitmarsh-Everiss, L. Laraia, *Nat. Chem. Biol.* **2021**, *17*, 653–664.
[19] J. Xiang, X. Liu, J. Ren, K. Chen, H. L. Wang, Y. Y. Miao, M. M. Qi, *Autophagy* **2019**, *15*, 197–211.
[20] P. Rühl, A. S. Rosato, N. Urban, S. Gerndt, R. Tang, C. Abrahamian, C. Leser, J. Sheng, A. Jha, G. Vollmer, M. Schaefer, F. Bracher, C. Grimm, *Sci. Rep.* **2021**, *11*, 1–14.
[21] X. Wu, J. Walker, J. Zhang, S. Ding, P. G. Schultz, *Chem. Biol.* **2004**, *11*, 1229–1238.
[22] A. Pahl, S. Sievers in *Systems Chemical Biology: Methods and Protocols* (Eds.: S. Ziegler, H. Waldmann), Springer, New York, **2019**, pp. 115-126.
[23] M. Grigalunas, A. Burhop, S. Zinken, A. Pahl, J. M. Gally, N. Wild, Y. Mantel, S. Sievers, D. J. Foley, R. Scheel, C. Strohmann, A. P. Antonchick, H. Waldmann, *Nat. Commun.* **2021**, *12*, 1883.
[24] L. Robke, Y. Futamura, G. Konstantinidis, J. Wilke, H. Aono, Z. Mahmoud, N. Watanabe, Y.-W. Wu, H. Osada, L. Laraia, H. Waldmann, *Chem. Sci.* **2018**, *9*, 3014–3022.
[25] M. Akbarzadeh, I. Deipenwisch, B. Schoelermann, A. Pahl, S. Sievers, S. Ziegler, H. Waldmann, *Cell Chem. Biol.* **2021**, *29*, 1053–1064 .
[26] A. Pahl, B. Schölermann, M. Rusch, M. Dow, C. Hedberg, A. Nelson, S. Sievers, H. Waldmann, S. Ziegler, *bioRxiv* preprint **2022**, 2022.08.15.503944.
[27] R. J. D'Amato, C. M. Lin, E. Flynn, J. Folkman, E. Hamel, *Proc. Natl. Acad. Sci. USA* **1994**, *91*, 3964–3968.
[28] R. Köchl, X. W. Hu, E. Y. W. Chan, S. A. Tooze, *Traffic* **2006**, *7*, 129–145.
[29] R. Mackeh, D. Perdiz, S. Lorin, P. Codogno, C. Poüs, *J. Cell Sci.* **2013**, *126*, 1071–1080.
[30] V. K. Gribkoff, J. E. Starrett, S. I. Dworetzky, P. Hewawasam, C. G. Boissard, D. A. Cook, S. W. Frantz, K. Heman, J. R. Hibbard, K. Huston, G. Johnson, B. S. Krishnan, G. G. Kinney, L. A. Lombardo, N. A. Meanwell, P. B. Molinoff, R. A. Myers, S. L. Moon, A. Ortiz, L. Pajor, R. L. Pieschl, D. J. Post-Munson, L. J. Signor, N. Srinivas, M. T. Taber, G. Thalody, J. T. Trojnacki, H. Wiener, K. Yeleswaram, S. W. Yeola, *Nat. Med.* **2001**, *7*, 471–477.
[31] D. Strøbæk, L. Teuber, T. D. Jørgensen, P. K. Ahring, K. Kjær, R. S. Hansen, S. P. Olesen, P. Christophersen, B. Skaaning-Jensen, *Biochim. Biophys. Acta Biomembr.* **2004**, *1665*, 1–5.
[32] X. Dai, Y. Liu, C. Wang, Y. Luo, X. Li, Z. Shen, *Biol. Pharm. Bull.* **2013**, *36*, 1583–1586.
[33] S. T. Granados, K. Castillo, F. Bravo-Moraga, R. V. Sepúlveda, W. Carrasquel-Ursulaez, M. Rojas, E. Carmona, Y. Lorenzo-Ceballos, F. González-Nilo, C. González, R. Latorre, Y. P. Torres, *Sci. Rep.* **2019**, *9*, 1–15.
[34] T. A. Roepke, A. Malyala, M. A. Bosch, M. J. Kelly, O. K. Rønnekleiv, *Endocrinology* **2007**, *148*, 4937–4951.
[35] X. Wu, S. Ding, Q. Ding, N. S. Gray, P. G. Schultz, *J. Am. Chem. Soc.* **2002**, *124*, 14520–14521.
[36] M. H. Woehrmann, W. M. Bray, J. K. Durbin, S. C. Nisam, A. K. Michael, E. Glassey, J. M. Stuart, R. S. Lokey, *Mol. BioSyst.* **2013**, *9*, 2604–2617.
[37] R. G. Sorensen, M. P. Blaustein, *Mol. Pharmacol.* **1989**, *36*, 689–698.

Manuscript received: September 21, 2022
Revised manuscript received: January 2, 2023
Accepted manuscript online: January 3, 2023
Version of record online: February 7, 2023